Sintering Process Simulation of Ag Nanoparticles by Phase Field Method

Hu, Xiao; Huang, Jianlin ; Poelma, René H.; van Driel, Willem Dirk; Zhang, Guoqi

DOI
10.1109/EuroSimE60745.2024.10491517

Publication date
2024

Document Version
Final published version

Published in
Proceedings of the 2024 25th International Conference on Thermal, Mechanical and Multi-Physics Simulation and Experiments in Microelectronics and Microsystems (EuroSimE)

Citation (APA)
Hu, X., Huang, J., Poelma, R. H., van Driel, W. D., & Zhang, G. (2024). Sintering Process Simulation of Ag Nanoparticles by Phase Field Method. In *Proceedings of the 2024 25th International Conference on Thermal, Mechanical and Multi-Physics Simulation and Experiments in Microelectronics and Microsystems (EuroSimE)* (2024 25th International Conference on Thermal, Mechanical and Multi-Physics Simulation and Experiments in Microelectronics and Microsystems, EuroSimE 2024). IEEE. https://doi.org/10.1109/EuroSimE60745.2024.10491517

2024 25th International Conference on Thermal, Mechanical and Multi-Physics Simulation and Experiments in Microelectronics and Microsystems (EuroSimE) | 979-8-3503-9363-7/24/$31.00 ©2024 IEEE | DOI: 10.1109/EuroSimE60745.2024.10491517

Sintering Process Simulation of Ag Nanoparticles by Phase Field Method

Xiao Hu[a,b,*], Jianlin Huang[b], René Poelma[c], Willem Dirk van Driel[a], Guoqi Zhang[a]
a. Delft University of Technology, Department of Microelectronics, Mekelweg 4, 2628 CD Delft, The Netherlands
b. Ampleon B.V., Halfgeleiderweg 8, 6534 AV Nijmegen, The Netherlands
c. Nexperia, Jonkerbosplein 52, 6534 AB Nijmegen, The Netherlands
Email: x.hu-1@tudelft.nl

Abstract

Low-temperature sintering technology of Ag nanoparticles is widely used in high-power electronic device packaging. Utilizing simulation methods to comprehend and control the microstructure and properties of Ag sintering materials has emerged as a prominent research area. This work uses the General Form PDE module in COMSOL to simplify the implementation of the phase field method. A two-particle model was established to explore the effects of different particle sizes and temperatures on the sintering neck of Ag nanoparticles. The two-particle model was expanded to multi-particle models and 3D models flexibly. This work presents the potential and limitations of these phase-field models, preparing for further multiphysics analysis and optimization of Ag sintering materials.

1. Introduction

Low-temperature sintering technology has been widely used in high-power device packaging in recent years, especially Silver (Ag) and Copper(Cu) sintering materials [1], [2], [3]. For instance, Ag sintering materials are composed of micro/nano-sized particles, allowing particles to be sintered at low temperatures (150 - 300 ^{o}C) below the melting point of bulk Ag (961 ^{o}C). The sintering process of nanoparticles involves complex diffusion effects at the nanoscale and is also affected by factors such as particle size, surface energy, temperature, and atmospheres [4], [5]. Understanding and controlling these processes is essential for adjusting the properties of metal sintering materials to suit various applications.

Simulation methods have become an indispensable tool for studying sintering processes and provide insights into multiscale sintering mechanisms from atomistic to macroscopic [6]. Molecular dynamics simulation is based on Newton's equations of motion, which can reveal the atomic-scale sintering mechanism from the atomic trajectories of particle diffusion and rotation [7], [8]. However, due to high computational costs, the size of nanoparticles is limited to a few nanometers to tens of nanometers.

At the microscopic level, the discrete elements method (DEM), Monte-Carlo method (MCM), and phase field method (PFM) have been used to simulate the sintering process. DEM is based on Newton's second law and rigid body dynamics so that it can describe interactions between a large number of particles, such as contact, collision, and fracture. While, DEM cannot take into account microstructural changes inside the particles during the sintering process [9], [10].

The Monte-Carlo method can capture pore migration and grain growth during sintering and is as applicable to multi-particle systems as DEM [11], [12]. It needs to define the interaction energy of different particle sites and the total energy of the system. The Metropolis algorithm is used to implement the random exchange between the site and adjacent sites so that its system evolves in the direction of reducing the total energy, such as the Q-state Potts model [13]. Due to this method's random sampling process, grain diffusion's randomness can be described, but the demand for computing resources is expensive.

The phase field method is a powerful tool based on thermodynamics for investigating phase transformations and microstructure evolution and is closer to the spatial and temporal scale of practical applications [14], [15]. In recent years, this method has received more attention from materials science and industrial applications. In this method, the sintering process under different conditions can be simulated by controlling parameters, which makes this method have certain versatility and flexibility [16], [17], [18]. This method has a more complex mathematical expression than other methods, with commonly utilized software including MOOSE, Pace3D, and others [19], [20].

This study focuses on simulating Ag nanoparticle sintering using the phase field method. By using the General Form Partial Differential Equation (PDE) module in COMSOL Multiphysics software [21], the mathematical implementation is simplified. A two-particle model was

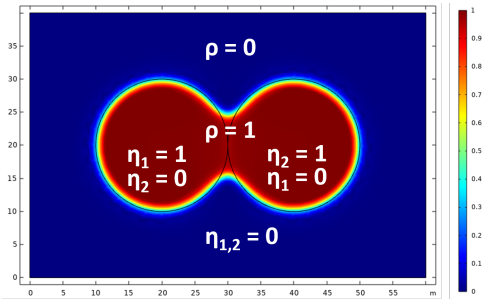

Figure 1. Schematic of phase field parameters setting in the two-particle model.

979-8-3503-9363-7/24/$31.00 ©2024 IEEE

established to explore the effects of different particle sizes and temperatures on the sintering neck of nanoparticles. This will pave the way for further combination with COMSOL multi-physics field analysis, and help the development and application of low-temperature nanoparticle sintering materials.

2. Methodology

A. Solid-state sintering by phase field method

In PFM, the sintering process is derived by minimizing the system's total free energy, F.

$$F = \int_V \left[f(\rho, \eta_{1\ldots i}) + \frac{\kappa_\rho}{2}(\nabla\rho)^2 + \sum_i \frac{\kappa_\eta}{2}(\nabla\eta_i)^2 \right] dV \quad (1)$$

where κ_ρ and κ_η are the gradient energy coefficients for concentration and grain boundary energies, respectively. The chemical free energy function $f(\rho, \eta_{1\ldots i})$ in **Equation (1)** is given by a Landau-type polynomial potential, as shown in **Equation (2)**, where A and B are model constants.

The phase field method uses two types of field variables to represent the microstructure. The first one is the conserved concentration field, denoted as ρ, following the Cahn-Hilliard equation:

$$\frac{\partial\rho}{\partial t} = \nabla \cdot \left(D\nabla \frac{\delta F}{\delta \rho} \right), \quad (3)$$

where D is the microstructure-dependent diffusivity. The conserved concentration field, ρ, takes 1 within the Ag particle and 0 outside the Ag particle, as shown in **Figure 1**.

The second is the non-conserved order parameter, η_i, which is used to distinguish the different particle types, following the Allen-Cahn Equation:

$$\frac{\partial\eta_i}{\partial t} = -L\frac{\delta F}{\delta \eta_i}. \quad (4)$$

L is the order parameter scalar mobility. In **Figure 1**, the i in η_i is used to denote different types of particles. The particle on the left is denoted as η_1 = 1, the particle on the right as η_2 = 1, and everywhere else, except the particle itself, as 0. There is no material property difference between η_1 and η_2 in this work, but it can be used to distinguish different particle crystal orientations or particle rotation directions in further work.

B. Implement two-particle model in COMSOL

The two-particle model of sintering simulation is an essential benchmark to establish the phase-field model successfully. The General Form PDE module in COMSOL was used to realize the simulation of the sintering process. The general equation form in this module is:

$$e_a\frac{\partial^2 \mathbf{u}}{\partial t^2} + d_a\frac{\partial \mathbf{u}}{\partial t} + \nabla\cdot\Gamma = \mathbf{f} \quad (5)$$

where e_a and d_a are mass coefficients, $\mathbf{u}$ is dependent variables. Γ is Conservative Flux, and $\mathbf{f}$ is Source Term.

In fact, **Equation (3)** is a fourth-order Cahn-Hilliard equation, so commonly split the equation into two second-order equations to fit the general equation form in this module, as Ref. ([22], [23]) did. Here, we introduce a field variable μ, and there are two second-order equations for the Cahn-Hilliard equation:

$$\frac{\partial\rho}{\partial t} = \nabla\cdot(D\nabla\mu), \quad (6)$$

$$\mu = \frac{\delta F}{\delta\rho} = \frac{\partial f}{\partial\rho} - \kappa_\rho\nabla^2\rho. \quad (7)$$

So we have 4 dependent variables, $\mathbf{u} = [\mu, \rho, \eta_1, \eta_2]^T$, and governing equations are:

$$\begin{cases} \nabla\cdot\left(\kappa_\rho\cdot\nabla\rho\right) = \frac{\partial f}{\partial\rho} - \mu \\ \frac{\partial\rho}{\partial t} - \nabla\cdot(D\cdot\nabla\mu) = 0 \\ \frac{\partial\eta_1}{\partial t} - \nabla(L\cdot\kappa_n\nabla\eta_1) = -L\frac{\partial f}{\partial\eta_1} \\ \frac{\partial\eta_2}{\partial t} - \nabla(L\cdot\kappa_n\nabla\eta_2) = -L\frac{\partial f}{\partial\eta_2} \end{cases} \quad (8)$$

In this way, the forms of the conserved flux and source terms are obvious.

According to the analysis in Ref. ([24], [25]), the relationship between parameters A, B, κ_ρ and κ_η in the total free energy F can be given as :

$$\begin{cases} \gamma_{sf} = \frac{\sqrt{2}}{6}\sqrt{\kappa_\rho+\kappa_\eta}\sqrt{A+7B} \\ \gamma_{gb} = \frac{2}{\sqrt{3}}\sqrt{B\kappa_\eta} \\ \delta_{gb} = \sqrt{\frac{4\kappa_\eta}{3B}} \end{cases} \text{or} \begin{cases} A = 12\frac{\gamma_{sf}}{\delta_{sf}} - 7\frac{\gamma_{gb}}{\delta_{gb}} \\ B = \frac{\gamma_{gb}}{\delta_{gb}} \\ \kappa_\rho = \frac{3}{2}\gamma_{sf}\delta_{sf} - \frac{3}{4}\gamma_{gb}\delta_{gb} \\ \kappa_\eta = \frac{3}{4}\gamma_{gb}\delta_{gb} \end{cases} \quad (9)$$

where γ_{gb}, γ_{sf}, δ_{gb} and δ_{sf} are the grain boundary energy, surface energy, grain boundary width, and surface width, respectively. These parameters are related to materials' properties, and their values are listed in **Table 1**. Normally, we assume $\delta_{gb} = \delta_{sf}$ as 2 nm. The order parameter scalar mobility L in **Equation (4)** can be defined as[26]:

$$L = \frac{\vartheta_{gb}\gamma_{gb}}{\kappa_\eta} \quad (10)$$

All model parameters we need are calculated and listed in **Table 2**.

All simulations were performed based on the physics-controlled mesh, with the element size set to "Finer" or better. Zero flux boundary conditions were applied at all four boundaries. The Time-Dependent study type with default settings was selected, and the implicit solver type and the default convergence criterion were adopted. The time step is 0.1 s, and different simulation durations are set according to specific cases. After the run, the concentration field is visualized.

2024 25th International Conference on Thermal, Mechanical and Multi-Physics Simulation and Experiments in Microelectronics and Microsystems (EuroSimE)

$$f(\rho,\eta_{1..p}) = A\rho^2\left(1-\rho^2\right) + B\left[\rho^2 + 6(1-\rho)\sum_i \eta_i^2 - 4(2\rho)\sum_i \eta_i^3 + 3\left(\sum_i \eta_i^2\right)^2\right] \quad (2)$$

Table 1. Materials properties for Ag

Propery	Value	Units	Ref.
ϑ_{gb}	10^{-16}	J m^4 J^{-1} s^{-1}	[27]
γ_{gb}	0.79	J m^{-2}	[28]
γ_{sf}	1.14	J m^{-2}	[29]
Q^{sf}	3.84×10^{-19}	J	[30]
D_o^{sf}	100	m^2 s^{-1}	[30]
Q^{vol}	3.15×10^{-19}	J	[27]
D_o^{vol}	0.67×10^{-4}	m^2 s^{-1}	[27]
D_{eff}^{gb}	$0.1D_{eff}^{sf}$		
D_{eff}^{vap}	$0.1D_{eff}^{vol}$		

Table 2. Model parameters in sintering phase field simulation

A	(kg/(nm·s^2))	B	(kg/(nm·s^2))	κ_ρ	(kg/(nm·s^2))
4.08		0.39		2.24	
κ_η	(kg/(nm·s^2))	L	(nm·s^2/kg)	γ_{sf}/γ_{gb}	(J/m^2)
1.19		6.64		1.44	

C. Materials parameters

In this section, parameters related to the material's properties are determined. In **Equation (3)**, D is assumed to be:

$$D = D_{vol}\varphi(\rho) + D_{vap}[1-\varphi(\rho)] + D_{sf}\rho(1-\rho) + D_{gb}\sum_i\sum_{i\neq m}\eta_i\eta_m. \quad (11)$$

where D_{vol} is the bulk diffusivity, D_{vap} is the diffusivity of vapour transport diffusivity, D_{sf} is the surface diffusivity, and D_{gb} is the grain boundary diffusivity. The interpolation function $\varphi(\rho)$ is taken as $\varphi(\rho) = \rho^3\left(10-15\rho+6\rho^2\right)$. The effective diffusivity obeys the Arrhenius equation:

$$D_{eff} = D_0 e^{-\frac{Q}{k_b T}} \quad (12)$$

where T is the temperature, k_b is Boltzmann constant, D_0 is a temperature-independent diffusivity and Q is the activation energy. According to **Table. 1** and **Equation (12)**, the effective diffusivity variation of Ag at different temperatures can be calculated as shown in **Figure 2**.

3. Results and Discussions

A. Size effect

The two-particle model simulated in COMSOL is compared with the result of the in-situ TEM experiment [31], as shown in **Figure 3**. The diameter of the simulated sintering neck length is smaller than the experimental result. θ is the dihedral angle between two particles, and it follows:

$$\gamma_{sf} = 2\gamma_{gb}cos\left(\frac{\theta}{2}\right). \quad (13)$$

As measured, the dihedral angle in **Figure 3(b)** is 76°. According to **Equation (13)**, γ_{sf}/γ_{gb} is 1.576, higher

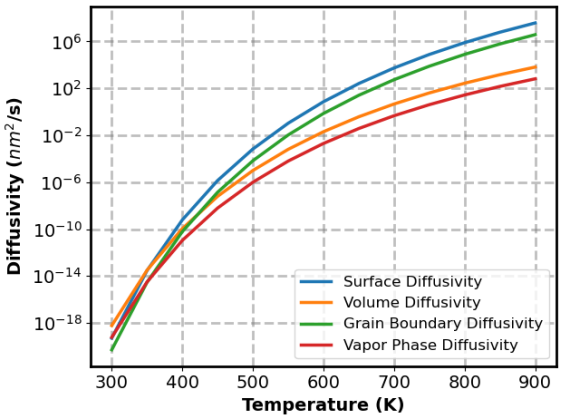

Figure 2. Effective diffusivity of Ag at different temperatures.

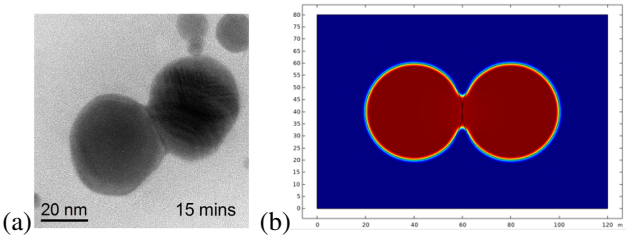

Figure 3. Stable sintered neck formed at 400°C of 40 nm particles in in-situ TEM of Ref.[31] (a), and that in phase field simulation (b).

than the preset value 1.44 in **Table 2**, which due to the gap between the adopted diffusivity at 400°C and the experimental data.

To investigate the size effect, we simulated the sintering process of the two-particle model with different diameters (20 nm, 40 nm, 80 nm) at 400°C as shown in **Figure 4**, and the changes of the sintering neck is recorded in **Figure 5**. The sintering neck X forms rapidly in the early stage of the sintering and increases slowly. At the same temperature, the larger the particle diameter D, the smaller the X/D ratio.This is because larger particles have smaller specific surface areas and require larger sintering driving force [5].

B. Temperature effect

The stable sintering neck of 20 nm particles at different temperatures(200 °C, 300 °C, 400 °C) are shown in **Figure 6**. The values of four diffusivities at different temperatures are listed in **Table 3**. The surface diffusivity of particls increases by 2 to 3 orders of magnitude when the temperature increases by 100 °C. It can be found that for particles of the same size, higher temperatures provide a higher diffusivity to promote the growth of the sintering

2024 25th International Conference on Thermal, Mechanical and Multi-Physics Simulation and Experiments in Microelectronics and Microsystems (EuroSimE)

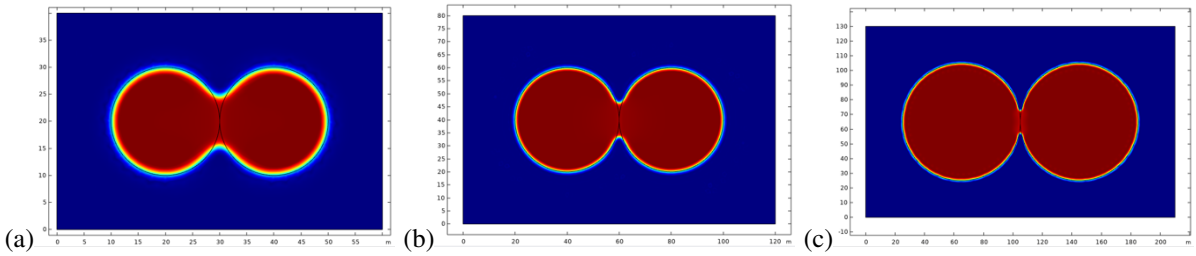

Figure 4. Stable sintered neck formed at 400°C of (a)particles with 20 nm diameter, (b) 40 nm diameter, and (c) 80 nm diameter.

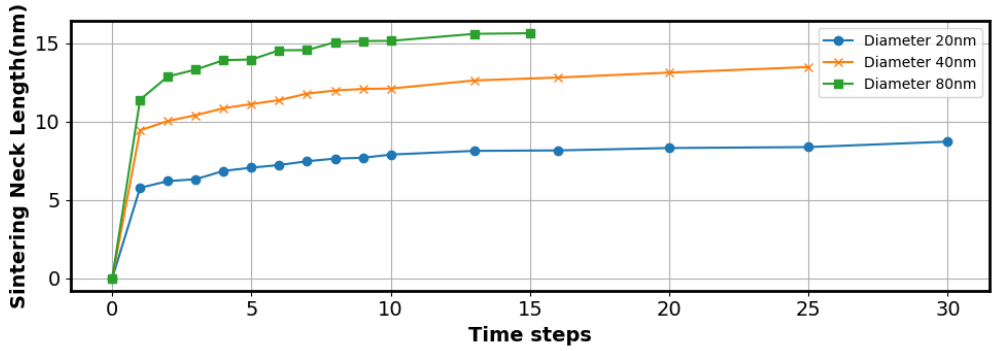

Figure 5. Changes of sintering neck for different particle diameters.

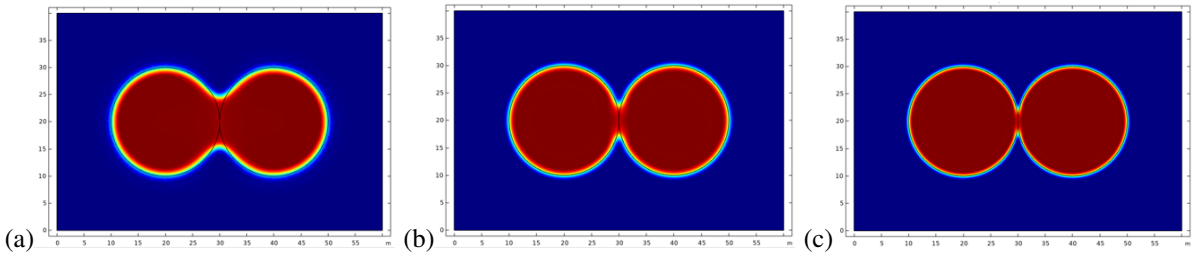

Figure 6. Stable sintered neck of particles with 20 nm diameter (a) sintering at 400°C, (b) 300°C, and (c)200°C.

Table 3. The effective diffusivity for Ag at different temperatures

Temperature (°C)	Surface Diffusivity $(\mathbf{nm}^2/\mathbf{s})$	Volume Diffusivity $(\mathbf{nm}^2/\mathbf{s})$	Grain Boundary $(\mathbf{nm}^2/\mathbf{s})$	Vapour Transport $(\mathbf{nm}^2/\mathbf{s})$
200	6.770×10^{-4}	9.991×10^{-6}	6.770×10^{-5}	9.991×10^{-7}
300	1.066×10^{-1}	6.339×10^{-4}	1.066×10^{-2}	6.339×10^{-5}
400	21.1	0.127	2.11	0.0127

neck, following the Arrhenius relationship.

C. Unequal-size particles

By adjusting the Geometry and increasing the model's dimensions in COMSOL, the two-particle model can be flexibly extended to the unequal-size particle model, the multi-particle model, and even the 3D sintering model.

In this unequal-size particle model as **Figure 7**, the original diameter of one particle is 20 nm, and the other is 10 nm. However, the two particles didn't melt into one circle particle. We attempted to consider the influence of the particle surface layer (thickness 1 nm) when modeling, as shown in **Figure 7(b)**, but the result is the same as that not adding a surface layer. According to the literature, the

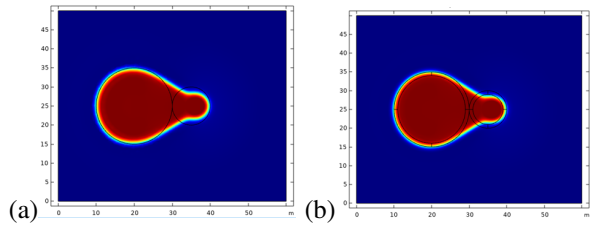

Figure 7. Stable sintering neck of two unequal-size particles. (a) No surface layer. (b) A 1 nm surface later.

reason could be the effect of surface projection tensor or not considering the rotation of particles during sintering [16], [17]. In future work, adjusting effective diffusivity

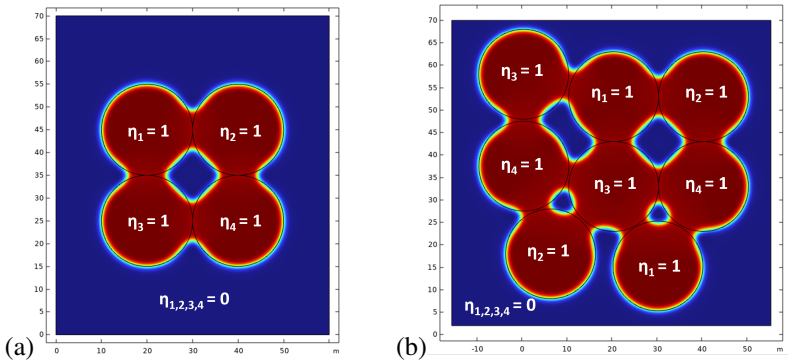

Figure 8. Stable sintering neck of (a) four-particle model, and (b) multiparticle model.

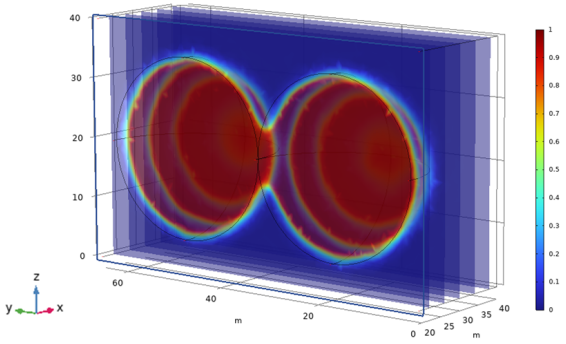

Figure 9. 3D two-particle model of sintering phase field simulation.

and considering particle rotation are solutions worth exploring.

D. Multiparticles

As for the multi-particle model as shown in **Figure 8(a)**, we added order parameters describing the type of particles, so that the dependent variable of this model is expanded to $\mathbf{u} = [\mu, \rho, \eta_1, \eta_2, \eta_3, \eta_4]^T$. Here, the diameter of all four particles is 20 nm, and the sintering neck is formed between two adjacent particles similar to that in the two-particle model as shown in **Figure 4(a)**. It is not necessary to use a separate order parameter description for each particle. As shown in **Figure 8(b)**, disconnected particles can also be described by the same order parameter, which in more complex models would mean that they have the same physical properties, such as crystal orientation or direction of translation or rotation. This can be seen as an advantage of the phase field method to simulate multi-particle systems flexibly.

E. 3D sintering model

Here, the two-particle model was extended to simulate the sintering process of 3D particles at 400 °C, as shown in **Figure 9**. All material parameter settings are consistent with the 2D two-particle model. The diameter of the 3D particles is 20 nm. In the 3D model, the section along the particle diameter shows the same sintering neck length as **Figure 4(a)**.

4. Conclusions

This study demonstrates the potential and limitations of implementing the phase field method by the general form PDE Module in COMSOL to simulate the sintering process of Ag nanoparticles. The size effect and temperature influence on the sintered microstructure are discussed using a two-particle model. And more complex multi-particle sintering models and 3D sintering models were implemented. We found that many factors affect sintering simulation, including particle geometry (equal or unequal), selected material property parameters (diffusivity, γ_{sf}/γ_{gb} ratio), and phase field model parameters (A, B, L, κ_ρ and κ_η).

At present, this model has not introduced the influence of particle translation and rotation during the sintering process. Moreover, we believe that it is worth discussing whether there are differences in microstructure evolution between 2D and 3D models. Further verification of the simulation through in-situ sintering experiments and parameter optimization is also advocated to provide a more accurate microstructure evolution, which will contribute to the development of Ag sintering materials and process optimization.

5. Acknowledgements

This publication is part of the Fundamentals of Backside Metals System project for 5G RF Power Modules, financed by the Dutch Research Council (NWO) under project No. 17969.

References

[1] Adeel Ahmad Bajwa, Yangyang Qin, Richard Reiner, Rudiger Quay, and Jurgen Wilde. Assembly and Packaging Technologies for High-Temperature and High-Power GaN Devices. *IEEE Transactions on Components, Packaging and Manufacturing Technology*, 5(10):1402–1416, October 2015.

[2] Seyed Amir Paknejad and Samjid H. Mannan. Review of silver nanoparticle based die attach materials for high power/temperature applications. *Microelectronics Reliability*, 70:1–11, March 2017.

[3] Kim S. Siow, editor. *Die-Attach Materials for High Temperature Applications in Microelectronics Packaging: Materials, Processes, Equipment, and Reliability*. Springer International Publishing, Cham, 2019.

[4] Conyers Herring. Effect of Change of Scale on Sintering Phenomena. *Journal of Applied Physics*, 21(4):301–303, April 1950.

[5] K. S. Siow and Y. T. Lin. Identifying the Development State of Sintered Silver (Ag) as a Bonding Material in the Microelectronic Packaging Via a Patent Landscape Study. *Journal of Electronic Packaging*, 138(020804), April 2016.

[6] Min Yi, Wenxuan Wang, Ming Xue, Qihua Gong, and Bai-Xiang Xu. Modeling and Simulation of Sintering Process Across Scales. *Archives of Computational Methods in Engineering*, 30(5):3325–3358, June 2023.

[7] Dong Hu, Zhen Cui, Jiajie Fan, Xuejun Fan, and Guoqi Zhang. Thermal kinetic and mechanical behaviors of pressure-assisted Cu nanoparticles sintering: A molecular dynamics study. *Results in Physics*, 19:103486, December 2020.

[8] Seunghwa Yang, Wonbae Kim, and Maenghyo Cho. Molecular dynamics study on the coalescence kinetics and mechanical behavior of nanoporous structure formed by thermal sintering of Cu nanoparticles. *International Journal of Engineering Science*, 123:1–19, February 2018.

[9] C. L. Martin, L. C. R. Schneider, L. Olmos, and D. Bouvard. Discrete element modeling of metallic powder sintering. *Scripta Materialia*, 55(5):425–428, September 2006.

[10] Weng-Hoh Lee, Yi Zhang, and Jing Zhang. Discrete element modeling of powder flow and laser heating in direct metal laser sintering process. *Powder Technology*, 315:300–308, June 2017.

[11] A. Luque, J. Aldazabal, A. MartÃn-Meizoso, J. M. MartÃnez-Esnaola, J. Gil Sevillano, and R. Farr. Simulation of the microstructural evolution during liquid phase sintering using a geometrical Monte Carlo model. *Modelling and Simulation in Materials Science and Engineering*, 13(7):1057, September 2005.

[12] Shihao Zhou, Xuhao Liu, Zilin Yan, Shotaro Hara, Naoki Shikazono, and Zheng Zhong. Kinetic Monte Carlo (KMC) simulation of sintering of nickel oxide-yttria stabilized zirconia composites: Model, parameter calibration and validation. *Materials & Design*, 232:112094, August 2023.

[13] Veena Tikare, Michael Braginsky, and Eugene A. Olevsky. Numerical Simulation of Solid-State Sintering: I, Sintering of Three Particles. *Journal of the American Ceramic Society*, 86(1):49–53, 2003. _eprint: https://ceramics.onlinelibrary.wiley.com/doi/pdf/10.1111/j.1151-2916.2003.tb03276.x.

[14] Johannes HÃ¶tzer, Marco Seiz, Michael Kellner, Wolfgang Rheinheimer, and Britta Nestler. Phase-field simulation of solid state sintering. *Acta Materialia*, 164:184–195, February 2019.

[15] S. Bulent Biner. *Programming Phase-Field Modeling*. Springer International Publishing, Cham, 2017.

[16] K. Chockalingam, V.G. Kouznetsova, O. van der Sluis, and M.G.D. Geers. 2D Phase field modeling of sintering of silver nanoparticles. *Computer Methods in Applied Mechanics and Engineering*, 312:492–508, December 2016.

[17] Sudipta Biswas, Daniel Schwen, and Vikas Tomar. Implementation of a phase field model for simulating evolution of two powder particles representing microstructural changes during sintering. *Journal of Materials Science*, 53(8):5799–5825, April 2018.

[18] Han Jiang, Shuibao Liang, Cheng Wei, and Changbo Ke. Phase field modelling of the electromigration behaviour in sintered silver. *Journal of Materials Research*, July 2022.

[19] Alexander D. Lindsay, Derek R. Gaston, Cody J. Permann, Jason M. Miller, David Andrš, Andrew E. Slaughter, Fande Kong, Joshua Hansel, Robert W. Carlsen, Casey Icenhour, Logan Harbour, Guillaume L. Giudicelli, Roy H. Stogner, Peter German, Jacob Badger, Sudipta Biswas, Leora Chapuis, Christopher Green, Jason Hales, Tianchen Hu, Wen Jiang, Yeon Sang Jung, Christopher Matthews, Yinbin Miao, April Novak, John W. Peterson, Zachary M. Prince, Andrea Rovinelli, Sebastian Schunert, Daniel Schwen, Benjamin W. Spencer, Swetha Veeraraghavan, Antonio Recuero, Dewen Yushu, Yaqi Wang, Andy Wilkins, and Christopher Wong. 2.0 - MOOSE: Enabling massively parallel multiphysics simulation. *SoftwareX*, 20:101202, 2022.

[20] J. HÃ¶tzer, A. Reiter, H. Hierl, P. Steinmetz, M. Selzer, and Britta Nestler. The parallel multi-physics phase-field framework Pace3D. *Journal of Computational Science*, 26:1–12, May 2018.

[21] COMSOL: Multiphysics Software for Optimizing Designs.

[22] Liangzhe Zhang, Michael R. Tonks, Derek Gaston, John W. Peterson, David Andrs, Paul C. Millett, and Bulent S. Biner. A quantitative comparison between c^0 and c^1 elements for solving the cahnâhilliard equation. *Journal of Computational Physics*, 236:74–80, March 2013.

[23] C.M. Elliott, D.A. French, and F.A. Milner. A second order splitting method for the Cahn-Hilliard equation. *Numerische Mathematik*, 54(5):575–590, 1989.

[24] Qingcheng Yang, Yongxin Gao, Arkadz Kirshtein, Qiang Zhen, and Chun Liu. A free-energy-based and interfacially consistent phase-field model for solid-state sintering without artificial void generation. *Computational Materials Science*, 229:112387, October 2023.

[25] K. Ahmed, C. A. Yablinsky, A. Schulte, T. Allen, and A. El-Azab. Phase field modeling of the effect of porosity on grain growth kinetics in polycrystalline ceramics. *Modelling and Simulation in Materials Science and Engineering*, 21(6):065005, July 2013. Publisher: IOP Publishing.

[26] N. Moelans, B. Blanpain, and P. Wollants. Quantitative analysis of grain boundary properties in a generalized phase field model for grain growth in anisotropic systems. *Physical Review B*, 78(2):024113, July 2008. Publisher: American Physical Society.

[27] S. J. Rothman, N. L. Peterson, and J. T. Robinson. Isotope Effect for Self-Diffusion in Single Crystals of Silver. *physica status solidi (b)*, 39(2):635–645, 1970.

[28] M. C. Inman and H. R. Tipler. Interfacial Energy and Composition in Metals and Alloys. *Metallurgical Reviews*, 8(1):105–166, January 1963.

[29] D. McLean and A. Maradudin. *Grain Boundaries in Metals*. *Physics Today*, 11(7):35–36, July 1958.

[30] G. E Rhead. Surface self-diffusion and faceting on silver. *Acta Metallurgica*, 11(9):1035–1042, September 1963.

[31] M.A. Asoro, P.J. Ferreira, and D. Kovar. In situ transmission electron microscopy and scanning transmission electron microscopy studies of sintering of Ag and Pt nanoparticles. *Acta Materialia*, 81:173–183, December 2014.